Title	Protolith identification of bedding-parallel, smectite-bearing shear zones in argillaceous and siliceous marine sediments; Discriminating between tephra-derived shear zones and host-rock-derived fault gouges
Author(s)	Ishii Eiichi
Citation	Engineering Geology,259,p.105203_1-105203_9
Text Version	Accepted Manuscript
URL	https://jopss.jaea.go.jp/search/servlet/search?5064299
DOI	https://doi.org/10.1016/j.enggeo.2019.105203
Right	© 2019. This manuscript version is made available under the CC-BY-NC-ND 4.0 license http://creativecommons.org/licenses/by-nc-nd/4.0/

Technical note

Protolith identification of bedding-parallel, smectite-bearing shear zones in argillaceous and siliceous marine sediments: discriminating between tephra-derived shear zones and host-rock-derived fault gouges

Eiichi Ishii

Horonobe Underground Research Center, Japan Atomic Energy Agency, Hokushin 432-2, Horonobe-cho, Hokkaido 098-3224, Japan

E-mail address: ishii.eiichi@jaea.go.jp

Abstract

Smectite-bearing shear zones are important in a variety of geoscientific and geoengineering fields owing to the unique physicochemical properties of smectite. Such shear zones occur globally in argillaceous and siliceous marine sediments, and are typically a product of either host-rock deformation, or exploitation of weak, altered tephra horizons within the sedimentary sequence. However, it is difficult to discriminate between a tephra-derived and host-rock-derived origin based on simple fault-rock observations. Here, a method is proposed that integrates two discriminators: the ratio of smectite to illite, sm/(ill + sm) (wt%/wt%), in the clay fractions of shear zone samples; and the ratio of conservative elements, Al_2O_3/TiO_2 (wt%/wt%), in the bulk chemistry of samples. Although high sm/(ill + sm) ratios may indicate a tephra-derived origin, deformation processes can lower the ratio, making protolith identification difficult. Previous studies have suggested that different Al_2O_3/TiO_2 ratios between shear zones and host rocks may also imply a tephra-derived origin. However, the Al_2O_3/TiO_2 ratios within shear zones may be intrinsically comparable with those of the host rock, even if the shear zones were derived from tephra layers. Despite these ambiguities, application of these two indicators to the protolith identification of bedding-parallel, smectite-bearing shear zones in a folded siliceous mudstone (Hokkaido, Japan) demonstrates that combining sm/(ill + sm) and Al_2O_3/TiO_2 ratios is a useful starting point when attempting to identify the protolith of smectite-bearing shear zones in argillaceous and siliceous marine mudstones.

Keywords

gouge, marine sediment, protolith, shear zone, smectite

1. Introduction

Tephra (volcanic ash) deposits are globally intercalated within argillaceous and siliceous marine sediments (Hein and Scholl, 1978; Compton, 1991; Delano et al., 1994). Under low-T diagenetic conditions, such tephra deposits undergo alteration to form smectite-bearing sedimentary horizons (Ross and Hendricks, 1945; Bradshaw, 1975; Compton, 1991), which are often subsequently exploited as shear zones during crustal deformation (Vrolijk, 1990; Kameda et al., 2015; Ishii and Furusawa, 2017). Smectite-bearing shear zones within argillaceous and siliceous marine sediments are of significant interest to both geoscientists and geoengineers working within the fields of structural geology, hydrogeology, and geochemistry, particularly those studying plate boundary faults (Vrolijk, 1990; Kameda et al., 2015, 2016), landslides (Bromhead, 2013; Massey et al., 2016), underground construction (Ishii et al., 2015; Ishii and Furusawa, 2017), and nuclear waste disposal (Iwatsuki et al., 2009; Murakami et al., 2016). This interest arises from the unique physicochemical properties of smectite, such as its low coefficient of friction, cation-exchange capacity, low permeability, expansivity, and variable consistency (Waltham, 2002). However, tephra-derived, smectite-bearing shear zones are similar in appearance to host-rock derived fault gouges, making it difficult to discriminate between them based on meso- and micro-scale observations alone (Ishii and Furusawa, 2017).

It is important to be discriminate between tephra-derived shear zones and host-rock-derived fault gouges because they typically differ with regard to their spatial extent and thickness, protolith mineralogy, and the time and process of formation, as well as their utility as marker beds (Ishii and Furusawa, 2017). For example, when a smectite-bearing shear zone is discovered in a pilot borehole at an investigation site and is shown (by mineralogy) to have a tephra-derived origin, the risk that a thick smectite-rich layer is extensively distributed around the borehole should be considered, even if the shear zone is very thin at the borehole. This risk arises because a tephra-derived shear zone is likely to be more extensive than a host-rock-derived fault gouge, and the thickness of the former may vary substantially, in part due to local stratigraphic pinchout of the original tephra layer. Therefore, discriminating tephra-derived shear zones and host-rock-derived fault gouges can provide knowledge of hazards (e.g., washout and groundwater inflow) caused by abundant smectite during underground construction (Ishii et al., 2015; Ishii and Furusawa, 2017), as well as their mitigation, by predicting the distribution of the shear zone based on that of the tephra layer. For distinguishing tephra-derived shear zones from host-rock-derived fault gouges, it is also important to ascertain the protolith mineralogy of shear zones, which is central to establishing thermal histories related to shear-zone seismicity (Kuo et al., 2009) and for studying the past migration of natural trace elements analogous to radionuclides of radioactive wastes (Iwatsuki et al., 2009). Knowledge of the origin of smectite-bearing shear zones also has application to the study of landslides (Bromhead, 2013).

Tephra-derived shear zones intrinsically have a higher smectite content than that of the surrounding host rock (Perry et al., 1976b; Vallier and Kidd, 1977; Tribble, 1990). Host-rock-derived fault gouges, on the other hand, are more likely to be mineralogically similar to the host rock (Holland et al., 2006). Thus, it should be possible to discriminate between the two by comparing the smectite content of the shear zone with that of the host rock. However, the smectite content in a tephra-derived shear zone may decrease over time as the shear zone becomes contaminated by host-rock materials during deformation. The smectite content may also decrease via syn-tectonic alteration, for example due to frictional heating during shear deformation (Yamaguchi et al., 2011; Schleicher et al., 2015; Kuo et al., 2016), or a combination of mechanical processes and chemical reactions (Vrolijk and Pluijm, 1999; Casciello et al., 2011; Hirono et al., 2014). Consequently, it is also difficult to discriminate between tephra-derived shear zones and host-rock-derived fault gouges by simply comparing their smectite content with that of the host rock.

This paper proposes a method utilizing two separate indicators as a means of confidently discriminating between tephra-derived shear zones and host-rock-derived fault gouges in argillaceous and siliceous marine sediments. The first indicator is the content of smectite normalised to that of illite (ill) plus smectite (sm) in the clay fraction of shear zone samples, defined as sm/(ill + sm) (wt%/wt%). The second indicator is the concentration of Al_2O_3 normalised to TiO_2 in the bulk chemistry of shear zone samples, defined as Al_2O_3/TiO_2 (wt%/wt%). Illite is a common clay mineral in argillaceous and siliceous marine sediments, so sm/(ill + sm) ratios are expected to be useful indicators in identifying protoliths of smectite-bearing shear zones. Based on previous studies, sm/(ill + sm) ratios of tephra-derived smectite-bearing layers are typically ≥ 0.9 (Perry et al., 1976a, b; Hein and Scholl, 1978; Tribble, 1990). However, with smectite content possibly decreasing over time due to deformation, the proportion of conservative elements (Al_2O_3/TiO_2) is also proposed. In argillaceous and siliceous marine sediments, the Al_2O_3/TiO_2 ratio of terrigenous detritus falls within a very narrow range (typically 22–24), as terrigenous material is homogenised during sedimentation, albeit without significant modification of certain original compositional features (Sugisaki et al., 1982; Yamamoto, 1984; Yamamoto et al., 1986). The Al_2O_3/TiO_2 ratios of volcanogenic materials, on the other hand, exhibit much wider ranges (10–130) and this characteristic remains even after alteration, although the range may reduce somewhat (to ~0.6 times the minimum ratio) (Yamamoto, 1984; Yamamoto et al., 1986). The Al_2O_3/TiO_2 ratio is thus expected to be useful in identifying the protolith of smectite-bearing shear zones.

To verify the feasibility of using the proposed method for the identification of the protolith of smectite-bearing shear zones, this study applied the method to bedding-parallel, clayey shear zones including soft clayey material intercalated within a Neogene siliceous mudstone in the Horonobe area, northern Hokkaido, Japan. Within this siliceous mudstone, numerous bedding-parallel slip surfaces have been developed by flexural-slip folding, with some being associated with clayey shear zones including soft clayey material (Ishii and Fukushima, 2006; Ishii, 2016; Hayano and Ishii, 2016; Ishii and Furusawa, 2017). Some of the clayey shear zones have already been found to be derived from tephra layers, via detailed mineralogical analyses of glass melt inclusions in mineral grains (Ishii and Furusawa, 2017). However, the protolith of some of the other clayey shear zones is still unknown.

In the siliceous mudstone, bedding-oblique slip surfaces are also developed (Ishii et al., 2010; Ishii, 2012) and are rarely associated with clayey shear zones, including soft clayey material observed in drill cores (Ishii, 2016; Ishii and Furusawa, 2017). However, the process of formation of soft clayey material in the bedding-oblique shear zones is not fully understood, and therefore such structures are unsuitable for verifying the proposed method. Thus, only bedding-parallel shear zones were investigated in the present study. Other types of clayey zone, unrelated to shear zones, have not been found in the siliceous mudstone.

2. Geological setting

The Horonobe area is located on the eastern margin of a Neogene–Quaternary sedimentary basin on the western side of northern Hokkaido, Japan. It is within an active Quaternary foreland fold-and-thrust belt, not far from the boundary between the Eurasian and North American plates (Fig. 1). From stratigraphically lowest to highest, the basin fill consists of the Masuporo, Wakkanai, Koetoi, Yuchi and Sarabetsu formations (Figs 1 and 2; note that the Masuporo Formation is not shown). The Wakkanai Formation, a Neogene siliceous mudstone, consists mainly of a single, massive, homogeneous lithofacies (Mitsui and Taguchi, 1977; Iijima and Tada, 1981), although weakly developed bedding planes are recognised in electrical-micro-imaging borehole logs (Ishii et al., 2006). As for the mineral composition, the mudstone comprises 40–50 wt% silica (mainly opal–cristobalite/tridymite: opal–CT), 19–33 wt% clay minerals (mainly smectite and illite), 9–13 wt% quartz, 7–13 wt% feldspar, 0–2 wt% pyrite, and 0–1 wt% carbonate (Mazurek and Eggenberger, 2005; Hiraga and Ishii, 2008). Although vitric tephra layers do not occur in the Wakkanai Formation, they are interbedded within the overlying diatomaceous mudstone containing biogenic opal-A (the Koetoi Formation, Figs 1 and 2) (Ishii et al., 2008).

Flexural folding of the Wakkanai Formation occurred between 2.2 and 1.0 Ma in response to regional E–W shortening, and subsequent uplift and denudation began at ~1 Ma (Ishii et al., 2008; Ishii, 2012). Displacements accrued along the bedding-parallel slip surfaces and clayey shear zones were contemporaneous with flexural-slip folding (Ishii and Fukushima, 2006; Ishii, 2016), with the displacements along the bedding-parallel slip surfaces inferred to be on the scale of decimetres or less (Ishii and Furusawa, 2017).

3. Samples and methods

Bedding-parallel, clayey shear zones including soft clayey material were identified through outcrop observations (Loc. 1 in Fig. 1), and by core logging and borehole wall image mapping in eight boreholes (HDB-1, -5, -6, -8, -9, -10, and -11, and PB-V01 in Fig. 1). The clayey shear zones have a maximum thickness of 30 cm, are light–dark grey in colour, and are associated with slip surfaces and/or fault breccias (Figs 3 and 4; Ishii, 2016; Ishii and Furusawa, 2017). Shear fabrics, such as S-foliations, were also confirmed within the shear zones and in the adjacent wall rocks during thin-section analyses (Ishii, 2016; Ishii and Furusawa, 2017); the S-foliations are typically highlighted by a scaly cleavage (Fig. 4b, c; Ishii, 2016; Ishii and Furusawa, 2017). Although the soft clayey material in shear zones are sticky when wet (Fig. 4d), the cracks highlighting the S-foliations may have been induced by desiccation of the core samples in the shear zones (Fig. 4a; Ishii 2016; Ishii and Furusawa, 2017) and in the adjacent wall rocks (Fig. 4e; Ishii, 2016). Clayey shear zones may be considered analogous to clay gouge (Vrolijk and Pluijm, 1999), but the term “gouge” may also indicate a mechanical formation process due to frictional wear or cataclasis (e.g., Engelder, 1974; Chester et al., 1985; Scholz, 1987). Because the process of formation of some of the clayey shear zones has not yet been determined, the term “clayey shear zones” is used to refer to discrete sheared layers composed of soft clayey material. This study also analysed bedding-parallel shear zones devoid of soft clayey material, for reference; although these zones do not contain soft clayey material, they are associated with slip surfaces that are lined with cohesive, scaly material (Fig. 4f–h).

Table 1 and Fig. 5 show details of the shear zone and host-rock samples that were analysed by X-ray diffraction (XRD) and X-ray fluorescence (XRF, for bulk chemical composition analyses). Samples collected from the outcrop at Loc. 1 were named using the format “KMH-X”, whereas the samples taken from drill cores were named according to the borehole from which they came (e.g., HDB-1) and the depth at which the samples were collected. For example, a sample taken from a depth of 599.4 m in borehole HDB-1 was given the name “HDB-1-599.4”. The soft clayey material, cohesive scaly material, and intact rock were sampled and analysed for the clayey shear zones, shear zones without soft clayey material, and host rock, respectively. Details of the analytical methods are provided below.

3.1. XRD analysis

The sm/(ill + sm) ratio for each sample was calculated from the relative proportions of smectite and illite, as determined by XRD analyses of ethylene-glycolated oriented powders. The relative proportions of smectite and illite that are used to determine the sm/(ill + sm) ratio should be the ratio of smectite to illite in smectite–illite mixed-layer clay species, considering that tephra-derived shear zones are expected to have abundant pure smectite (Perry and Hower, 1970; Perry et al., 1976a, b; Hein and Scholl, 1978). However, the method of determining the ratio of smectite to illite in smectite–illite mixed-layer clay species using the peak positions in XRD profiles might not be suitable for mudstone, as detrital illite may mask those peak positions (Reynolds and Hower, 1970; Rettke, 1981). Although using the saddle peak on the low-angle side of the 17 Å peak for smectite is also useful (Rettke, 1981; Inoue et al., 1989), this method has not yet been routinely incorporated as a standard practice, including for determining the baseline of intensity in the XRD profiles, and there is a lack of associated analytical software. In the present study, as a conventional and practical method, the relative proportions of the basal peak areas for smectite and illite in the glycolated oriented samples were used and were weighted according to the method of Biscaye (1965); i.e., using the area of the 17 Å peak for smectite and four times (4 ×) the 10 Å peak area for illite. This weighting method has a maximum analytical error of 20 wt% (Underwood et al., 1993). As pointed out by Rettke (1981), the 17 Å peak can include both the peaks of discrete smectite and of smectite–illite mixed-layer clay, and the 10 Å peak can include both the peaks of discrete illite and of smectite–illite mixed-layer clay. Thus, the ratio of smectite to illite calculated from the ratio of those peak areas does not directly express the ratio of smectite to illite in smectite–illite mixed-layer clay species. However, a difference in the ratio of smectite to illite in smectite–illite mixed-layer clay may resultantly appear as a difference in the ratio of the 17 Å peak area to the 10 Å peak area (Rettke, 1981), and such a trend can be confirmed in numerous data previously reported (Hein & Scholl 1978; Tribble 1990; Guo and Underwood, 2012). Thus, the present study employed the ratio of the 17 Å peak area to the 10 Å peak area as an alternative indicator of the ratio of smectite to illite in smectite–illite mixed-layer clay, and the sm/(ill + sm) ratios were determined on the basis of those peak areas.

Some of the XRD analyses were performed at the Hiruzen Institute for Geology and Chronology, using a RIGAKU Rint-2500V diffractometer under the following conditions: target = Cu; voltage = 40 kV; current = 160 mA; scan speed = 4° min^{-1}. Other analyses were conducted at Earth Science Co. Ltd., Japan, using a Shimadzu XRD-6000 diffractometer under the following conditions: target = Cu; voltage = 30 kV; current = 20 mA; scan speed = 2° min^{-1}.

3.2. XRF analysis

The Al_2O_3/TiO_2 ratio for each sample was determined using the Al_2O_3 and TiO_2 values yielded by XRF analyses. The XRF analyses were performed by ALS Canada Ltd., using a sequential wavelength dispersive XRF spectrometer (PANalytical Axios). The limit of detection (LOD) for each element in the XRF determinations was 0.01 wt%.

4. Results and discussion

Fig. 6 shows the sm/(ill + sm) ratios of the samples. The values for clayey shear zones are ~0.2–1.0, whereas those of host-rock samples are ~0.1–0.6 (Fig. 6). The Δ2θ value between the peak positions of illite (001)/smectite (002) and illite (002)/smectite (003) was close to 5.3° for the clayey shear-zone samples that exhibited the highest sm/(ill + sm) ratios (≥0.9) (Fig. 7a). This indicates that the smectite-bearing minerals in these samples are almost pure smectite (Watanabe, 1988). This interpretation is consistent with the size of the saddle peaks (Rettke, 1981; Inoue et al., 1989) on the low-angle side of the 17 Å peak (5° 2θ, 001 peak) for the smectite in those samples, whereby the saddle/001 peak intensity ratios are very small compared with those of samples exhibiting lower sm/(ill + sm) ratios (Fig. 7). Such pure smectite indicates a tephra-derived origin, and thus the samples with sm/(ill + sm) values of ≥0.9 can be inferred to have been derived from tephra layers (Perry et al., 1976a, b; Hein and Scholl, 1978; Tribble, 1990). The samples with sm/(ill + sm) values of ~0.7–0.9 also have higher sm/(ill + sm) ratios than the host rock samples, and thus are also inferred to have been derived from tephra layers. It is suggested that their sm/(ill + sm) ratios have decreased from ≥0.9 to ~0.7–0.9 by mineralogical disturbance and/or alteration during shear deformation (e.g., contamination with the host rock materials, and/or syn-tectonic alteration). The sm/(ill + sm) ratios determined for the bedding-parallel shear zones devoid of soft clayey material are similar to those of the host rock (Fig. 6).

Integration of the sm/(ill + sm) and Al_2O_3/TiO_2 data shows that Al_2O_3/TiO_2 ratios of the clayey shear samples with sm/(ill + sm) ratios of ≥0.7 range widely from ~19 to ~92, whereas Al_2O_3/TiO_2 ratios of the clayey shear zone samples with sm/(ill + sm) ratios of <0.7 fall into a much narrower range of ~22–25, which is close to the range (~21–22) of host-rock samples (Fig. 6). These patterns are observed regardless of the instrument or XRD settings (Fig. 6). Considering that the clayey shear zones with sm/(ill + sm) ratios of ≥0.7 are inferred to have been derived from tephra layers, the distinct ranges of Al_2O_3/TiO_2 values suggest that they can be used to identify the protolith of bedding-parallel, clayey shear zones in argillaceous and siliceous marine sediments; i.e., clayey shear zone samples with Al_2O_3/TiO_2 ratios different from those of the host rock are inferred to be derived from tephra layers, as suggested previously (Yamamoto, 1984; Yamamoto et al., 1986). However, in some cases the Al_2O_3/TiO_2 ratios of clayey shear zones may intrinsically be the same as those of the host rock, even when shear zones are derived from tephra layers, as shown by some samples in Fig. 6 with sm/(ill + sm) ratios of ≥0.7 (Yamamoto, 1984; Yamamoto et al., 1986). Al_2O_3/TiO_2 ratios of the bedding-parallel shear zones devoid of soft clayey material are similar to those of the host rock (Fig. 6).

Although the five samples with sm/(ill + sm) ratios of <0.7 (KMH-4, HDB-6-458.4, HDB-9-104.5, HDB-10-434.6, and PB-V01-285.5) have Al_2O_3/TiO_2 ratios close to those of the host-rock samples, the Al_2O_3/TiO_2 ratios of samples KMH-4, HDB-10-434.6, and PB-V01-285.5 (24.52, 23.92, and 24.33, respectively; Table 1) are slightly higher than the maximum value (22.43) of host-rock samples (Fig. 6). Although this difference appears to be slight, it may be of significance considering the very small measurement error (LOD = 0.01 wt%) of XRF analyses. It is therefore proposed that the clayey shear zones from which these three samples were taken were also originally derived from tephra layers and that their sm/(ill + sm) ratios decreased from ≥0.9 to <0.7 via mineralogical disturbance and/or alteration during shear deformation. The clayey shear zones associated with samples HDB-6-458.4 and HDB-9-104.5 have sm/(ill + sm) and Al_2O_3/TiO_2 ratios that are comparable with those of the host rock (Fig. 6). It is therefore not possible to determine whether these two shear zones are derived from tephra or host rock based solely on the sm/(ill + sm) and Al_2O_3/TiO_2 ratios.

Ishii (2016), using detailed microscopic, mineralogical and geochemical analyses, attributed the evolution of the clayey shear zone from which sample HDB-10-434.6 was taken to shear deformation of the host rock; however, it was not clear why shear deformation was initially localised within that particular horizon. The results outlined above suggest that the horizon may have originated as a thin, altered tephra layer, which was exploited as a plane of weakness during shear deformation, and subsequently evolved into a broader, clayey shear zone.

Identification of the protolith of bedding-parallel smectite-bearing shear zones in argillaceous and siliceous marine sediments is typically difficult, as the nature of the protolith is largely lost via diagenesis and/or mineralogical disturbances and alteration during shear deformation. However, the method proposed in this paper, based on the integration of two indicators, sm/(sm + ill) and Al_2O_3/TiO_2 ratios, is relatively simple to implement and may be a useful starting point when attempting such discriminations. Although high sm/(ill + sm) ratios may indicate a tephra-layer origin, the ratios are susceptible to distortion by both deformation processes and XRD analytical errors. Shear-zone samples yielding Al_2O_3/TiO_2 ratios that differ from those of the host rock can also be used as evidence that the shear zone was initially derived from a tephra horizon. In that case, the data are unlikely to be affected by small measurement errors associated with XRF analyses, but the Al_2O_3/TiO_2 ratio may be intrinsically similar to that of the host rock, even if the shear zones were derived from tephra layers. Both the proposed indicators thus have their own pros and cons, but integration of the two may facilitate the identification of the protolith of clayey shear zones in argillaceous and siliceous marine mudstones.

Finally, it is noted that the applicability of the proposed method also depends on the lithological heterogeneity of the host rock and the amount of pure smectite in the host rock. The investigated host rock is a quite massive, lithologically homogeneous mudstone that yields Al_2O_3/TiO_2 ratios of ~21–22 (Fig. 6; Table 1), which are inferred to correspond to the Al_2O_3/TiO_2 ratio of terrigenous detritus that is homogeneously distributed throughout the host rock. Pure smectite is also not particularly abundant, and the sm/(ill + sm) ratio is <0.7 (Fig. 6; Table 1). However, if a host rock were highly heterogeneous in lithofacies and contained a high concentration of detrital/authigenic pure smectite due to specific sedimentation conditions (e.g., Kameda et al., 2015) rather than to particular ash fall events, it might be difficult to discriminate between tephra-derived shear zones and host-rock-derived fault gouges, as the resultant sm/(ill + sm) ratios might be very similar.

5. Conclusions

Samples of bedding-parallel, clayey shear zones intercalated within a folded siliceous mudstone, plus host rock samples, were analysed using XRD and XRF to evaluate the feasibility of using sm/(ill + sm) and Al_2O_3/TiO_2 ratios as a tool for identifying the protolith of bedding-parallel, clayey shear zones in argillaceous and siliceous marine sediments, with results as follows.

- Tephra-derived shear zones were detected by their sm/(ill + sm) ratios, which were higher than those of the host rock; most of them also exhibited different Al_2O_3/TiO_2 ratios to those of the host rock. This suggests that both sm/(ill + sm) and Al_2O_3/TiO_2 ratios can be useful indicators of the protolith of smectite-bearing shear zones.
- Although some clayey shear zones exhibited sm/(ill + sm) ratios similar to those of the host rock, they were also inferred to be derived from tephra layers, as their Al_2O_3/TiO_2 values differed from those of the host rock.
- The method applied in this study represents a viable initial evaluation tool when attempting to identify the protolith of smectite-bearing shear zones in argillaceous and siliceous marine sediments.

Acknowledgements

The author thanks T. Murakami for valuable input regarding the bulk chemistry of the clayey shear zones, A. Hayano for helpful assistance in sampling KMH-3 and KMH-4, two anonymous reviewers for valuable comments, and A. Stallard for improving the grammar and for helpful suggestions regarding the manuscript.

Fig. 1 Geological map and cross-section of the Horonobe area (after Ishii, 2012), showing the locations of boreholes and the outcrop illustrated in Fig. 3.

Fig. 2 Schematic columnar section through the stratigraphy in the Horonobe area (Ishii et al., 2010), including lithological descriptions of the main stratigraphic units. Sb = Sarabetsu Formation; Yc = Yuchi Formation; Kt = Koetoi Formation; Wk = Wakkanai Formation.

Fig. 3 Photographs of bedding-parallel, clayey shear zones and bedding-parallel slip surfaces devoid of soft clayey material exposed in outcrop (the location of the outcrop is shown in Fig. 1). (a, b) KMH-1 and KMH-2; (c) KMH-3; (d) KMH-4; and (e) KMH-4.

Fig. 4 (a) Photograph of the bedding-parallel, clayey shear zone with the greatest thickness (HDB-1-432.9). The sample was taken from the ~5 cm thick, light-grey bottom layer. (b, c) Photographs of typical bedding-parallel, clayey shear zones (HDB-6-444.6 and PB-V01-285.5). (d) Photograph of sticky, clayey material within the bedding-parallel, clayey shear zone of PB-V01-395.8. (e) Photograph of desiccation cracks highlighting an S-foliation observed in the hanging wall of the bedding-parallel, clayey shear zone of PB-V01-472.0. (f) Photograph of a bedding-parallel shear zone without soft clayey material but exhibiting cohesive scaly material (HDB-6-445.6). (g, c) Photographs of a bedding-parallel shear zone without soft clayey material (HDB-11-883.5). Cohesive scaly material is observed on the footwall slip surface.

Fig. 5 Borehole logs summarising the stratigraphic distribution of bedding-parallel, clayey shear zones and tephra layers (modified from Ishii and Furusawa, 2017). For numbers with the format XXX.X(Y), XXX.X refers to the depth of occurrence (metres below ground level) and Y refers to the thickness (centimetres). Data relating to tephra layers are from Ishii et al. (2008). *Not analysed in this study, due to insufficient sample.

Fig. 6 Al_2O_3/TiO_2 vs sm/(ill + sm) diagram for the analysed samples. * sm/(ill + sm) ratios based on XRD determinations performed by the Hiruzen Institute for Geology and Chronology (this study); ** sm/(ill + sm) ratios based on XRD determinations performed by Earth Science Co. Ltd. (this study); *** sm/(ill + sm) ratios from Milodowski et al. (2004). BPSZ = Bedding-parallel shear zone.

Fig. 7 Ethylene-glycolated XRD profiles of: (a, b) the bedding-parallel, clayey shear zones of HDB-6-444.6 and PB-V01-285.5; (c) the bedding-parallel shear zone without soft clayey material of HDB-11-883.5; and (d) the host rock of PB-V01-396.0.

Table 1 Details of and analytical results for the shear zone and host rock samples analysed in this study.

References

Biscaye, P.E., 1965. Mineralogy and sedimentation of recent deep-sea clays in the Atlantic Ocean and adjacent seas and oceans. Geological Society of America Bulletin 76, 803–832.

Bradshaw, M.J., 1975. Origin of montmorillonite bands in the middle Jurassic of eastern England. Earth and Planetary Science Letters 26, 245–252.

Bromhead, E.N., 2013. Reflections on the residual strength of clay soils, with special reference to bedding-controlled landslides. Quarterly Journal of Engineering Geology and Hydrogeology 46, 132–155.

Casciello, E., Cosgrove, J.W., Cesarano, M., Romero, E., Queralt, I., Vergés, J., 2011. Illite-smectite patterns in sheared Pleistocene mudstones of the Southern Apennines and their implications regarding the process of illitization: a multiscale analysis. Journal of Structural Geology 33, 1699–1711.

Chester, F.M., Friedman, M., Logan, J.M., 1985. Foliated cataclasites. Tectonophysics 111, 139–146.

Compton, J.S., 1991. Origin and diagenesis of clay minerals in the Monterey Formation, Santa Maria basin area, California. Clays and Clay Minerals 39, 449–466.

Delano, J.W., Tice, S.J., Mitchell, C.E., Goldman, D., 1994. Rhyolitic glass in Ordovician K-bentonites: a new stratigraphic tool. Geology 22, 115–118.

Engelder, J.T., 1974. Cataclasis and the generation of fault gouge. Geological Society of America Bulletin 85, 1515–1522.

Guo, J., Underwood, M.B., 2012. Data report: clay mineral assemblages from the Nankai Trough accretionary prism and the Kumano Basin, IODP Expeditions 315 and 316, NanTroSEIZE Stage. Proceedings of the Integrated Ocean Drilling Program 314/315/316, doi:10.2204/iodp.proc.314315316.202.2012.

Hayano, A., Ishii, E., 2016. Relationship Between Faults Oriented Parallel and Oblique to Bedding in Neogene Massive Siliceous Mudstones at The Horonobe Underground Research Laboratory, Japan. In: IOP Conference Series: Earth and Environmental Science. 44, 022004. http://dx.doi.org/10.1088/1755-1315/44/2/022004.

Hein, J.R., Scholl, D.W., 1978. Diagenesis and distribution of late Cenozoic volcanic sediment in the southern Bering Sea. Geological Society of America Bulletin 89, 197–210.

Hiraga, N., Ishii, E., 2008. Mineral and Chemical Composition of Rock Core and Surface Gas Composition in Horonobe Underground Research Laboratory Project (Phase 1). Japan Atomic Energy Agency, Tokai-mura, Japan JAEA Technical Report JAEA-Data/Code 2007-022.

Hirono, T., Ishikawa, T., Masumoto, H., Kameda, J., Yabuta, H., Mukoyoshi, H., 2014. Re-evaluation of frictional heat recorded in the dark gouge of the shallow part of a megasplay fault at the Nankai Trough. Tectonophysics 626, 157–169.

Holland, M., Urai, J.L., van der Zee, W., Stanjek, H., Konstanty, J., 2006. Fault gouge evolution in highly overconsolidated claystones. Journal of Structural Geology 28, 323–332.

Iijima, A., Tada, R., 1981. Silica diagenesis of Neogene diatomaceous and volcaniclastic sediments in northern Japan. Sedimentology 28, 185–200.

Inoue, A., Bouchet, A., Velde, B., Meunier, A., 1989. Convenient technique for estimating smectite layer percentage in randomly interstratified illite/smectite minerals. Clays and Clay Minerals 37, 227–234.

Ishii, E., 2012. Microstructure and origin of faults in siliceous mudstone at the Horonobe Underground Research Laboratory site, Japan. Journal of Structural Geology 34, 20–29.

Ishii, E., 2016. The role of bedding in the evolution of meso- and microstructural fabrics in fault zones. Journal of Structural Geology 89, 130–143.

Ishii, E., Fukushima, T., 2006. A case study of analysis of faults in Neogene siliceous rocks. Journal of the Japan Society of Engineering Geology 47, 280–291.

Ishii, E., Furusawa, A., 2017. Detection and correlation of tephra-derived smectite-rich shear zones by analyzing glass melt inclusions in mineral grains. Engineering Geology 228, 158–166.

Ishii, E., Yasue, K., Tanaka, T., Tsukuwi, R., Matsuo, K., Sugiyama, K., Matsuo, S., 2006. Three-dimensional distribution and hydrogeological properties of the Omagari Fault in the Horonobe area, northern Hokkaido, Japan. The Journal of the Geological Society of Japan 112, 301–314.

Ishii, E., Yasue, K., Ohira, H., Furusawa, A., Hasegawa, T., Nakagawa, M., 2008. Inception of anticline growth near the Omagari Fault, northern Hokkaido, Japan. The Journal of the Geological Society of Japan 114, 286–299.

Ishii, E., Funaki, H., Tokiwa, T., Ota, K., 2010. Relationship between fault growth mechanism and permeability variations with depth of siliceous mudstones in northern Hokkaido, Japan. Journal of Structural Geology 32, 1792–1805.

Ishii, E., Hashimoto, Y., Inagaki, D., 2015. Washout of clay-rich gouge in a pre-grouted fault zone and increase in groundwater inflow during tunnel excavation in Neogene siliceous mudstone (Horonobe, Japan). In: Proceedings 10th Asian Regional Conference of IAEG. Japan Society of Engineering Geology pp. 1–4 Tp3-P02.

Iwatsuki, T., Ishii, E., Mizuno, T., Honda, T., 2009. Natural analogue study on trace element migration in geological formation at Horonobe area, Japan. Bulletin of Atomic Energy Research Laboratory Tokyo City University 32, 1–13.

Kameda, J., Inaoi, C., Conin, M., 2016. Exchangeable cation composition of the smectite-rich plate boundary fault at the Japan Trench. Geophysical Research Letters 43, 3112–3119.

Kameda, J., Shimizu, M., Ujiie, K., Hirose, T., Ikari, M., Mori, J., Oohashi, K., Kimura, G., 2015. Pelagic smectite as an important factor in tsunamigenic slip along the Japan Trench. Geology 43, 155–158.

Kuo, L.-W., Song, S.-R., Yeh, E.-C., Chen, H.-F., 2009. Clay mineral anomalies in the fault zone of the Chelungpu Fault, Taiwan, and their implications. Geophysical Research Letters 36, L18306.

Kuo, L.-W., Song, S.-R., Suppe, J., Yeh, E.-C., 2016. Fault mirrors in seismically active fault zones: A fossil of small earthquakes at shallow depths. Geophysical Research Letters 43, 1950–1959.

Massey, C.I., Petley, D.N., McSaveney, M.J., Archibald, G., 2016. Basal sliding and plastic deformation of a slow, reactivated landslide in New Zealand. Engineering Geology 208, 11–28.

Mazurek, M., Eggenberger, U., 2005. Mineralogical analysis of core samples from the Horonobe area. Institute of Geological Sciences, University of Bern, Switzerland RWI Technical Report 05-01.

Milodowski, A.E., Barnes, R.P., Bouch, J., Kemp, S.J., Wagner, D., 2004. Characterisation of fractured rock and fracture mineralisation in Horonobe Boreholes HDB-6, HDB-7 and HDB-8: Final Report. British Geological Survey, Keyworth Nottingham, UK Commissioned Report CR/04/251.

Mitsui, K., Taguchi, K., 1977. Silica mineral diagenesis in Neogene tertiary shales in the Tempoku district, Hokkaido, Japan. Journal of Sedimentary Petrology 47, 158–167.

Murakami, T., Sasamoto, H., Mizuno, T., 2016. Retention of rare earth elements, thorium and uranium in sedimentary rocks: a case study in the Horonobe area of Hokkaido, Japan. Chikyukagaku 50, 1–19.

Perry, E., Hower, J., 1970. Burial diagenesis in Gulf Coast pelitic sediments. Clays and Clay Minerals 18, 165–177.

Perry, E., Beckles, E.C., Newton, R.M., 1976a. Chemical and mineralogical studies, sites 322 and 325. In: Hollister, C.D., Craddock, C., et al. (Eds.), Init. Repts. DSDP. U. S. Govt. Printing Office, Washington, pp. 465–469.

Perry, E.A., Gieskes, J.M., Lawrence, J.R., 1976b. Mg, Ca and O^{18}/O^{16} exchange in the sediment-pore water system, Hole 149, DSDP. Geochimica et Cosmochimica Acta 40, 413–423.

Rettke, R.C., 1981. Probable burial diagenetic and provenance effects on Dakota group clay mineralogy, Denver basin. Journal of Sedimentary Petrology 51, 541–551.

Reynolds, R.C., Hower, J., 1970. The nature of interlayering in mixed-layer illite-montmorillonite. Clays and Clay Minerals 18, 25–36.

Ross, C.S., Hendricks, S.B., 1945. Minerals of the Montmorillonite Group: Their Origin and Relation to Soils and Clays. US Government Printing Office, Washington.

Schleicher, A.M., Boles, A., van der Pluijm, B.A., 2015. Response of natural smectite to seismogenic heating and potential implications for the 2011 Tohoku earthquake in the Japan Trench. Geology 43, 755–758.

Scholz, C.H., 1987. Wear and gouge formation in brittle faulting. Geology 15, 493–495.

Sugisaki, R., Yamamoto, K., Adachi, M., 1982. Triassic bedded cherts in central Japan are not pelagic. Nature 298, 644–647.

Tribble, J.S., 1990. Clay diagenesis in the Barbados accretionary complex: Potential impact on hydrology and subduction dynamics. Proceedings Ocean Driling Program Scientific Results 110, 97–110.

Underwood, M.B., Orr, R., Pickering, K., Taira, A., 1993. Provenance and dispersal patterns of sediments in the turbidite wedge of Nankai trough. Proceedings of the Ocean Drilling Program Scientific Results 131, 15–34.

Vallier, T.L., Kidd, R.B., 1977. Volcanogenic sediments in the Indian Ocean. In: Heirtzler, J.R., Bolli, H.M., Davies, T.A., Saunders, J.B., Sclater, J.G. (Eds.), Indian Ocean Geology and Biostratigraphy. American Geophysical Union, Washington, pp. 87–118.

Vrolijk, P., 1990. On the mechanical role of smectite in subduction zones. Geology 18, 703–707.

Vrolijk, P., van der Pluijm, B.A., 1999. Clay gouge. Journal of Structural Geology 21, 1039–1048.

Waltham, T., 2002. Foundations of Engineering Geology, Second edition. Spon Press, New York.

Watanabe, T., 1988. The structural model of illite/smectite interstratified mineral and the diagram for its identification. Clay Science 7, 97–114.

Yamaguchi, A., Sakaguchi, A., Sakamoto, T., Iijima, K., Kameda, J., Kimura, G., Ujiie, K., Chester, F.M., Fabbri, O., Goldsby, D., Tsutsumi, A., Li, C.-F., Curewitz, D., 2011. Progressive illitization in fault gouge caused by seismic slip propagation along a megasplay fault in the Nankai Trough. Geology 39, 995–998.

Yamamoto, K., 1984. Geochemical study of acidic tuffs and siliceous shales from the Setogawa Terrane in the western part of Shizuoka City. The Journal of the Geological Society of Japan 90, 479–496.

Yamamoto, K., Sugisaki, R., Arai, F., 1986. Chemical aspects of alteration of acidic tuffs and their application to siliceous deposits. Chemical Geology 55, 61–76.

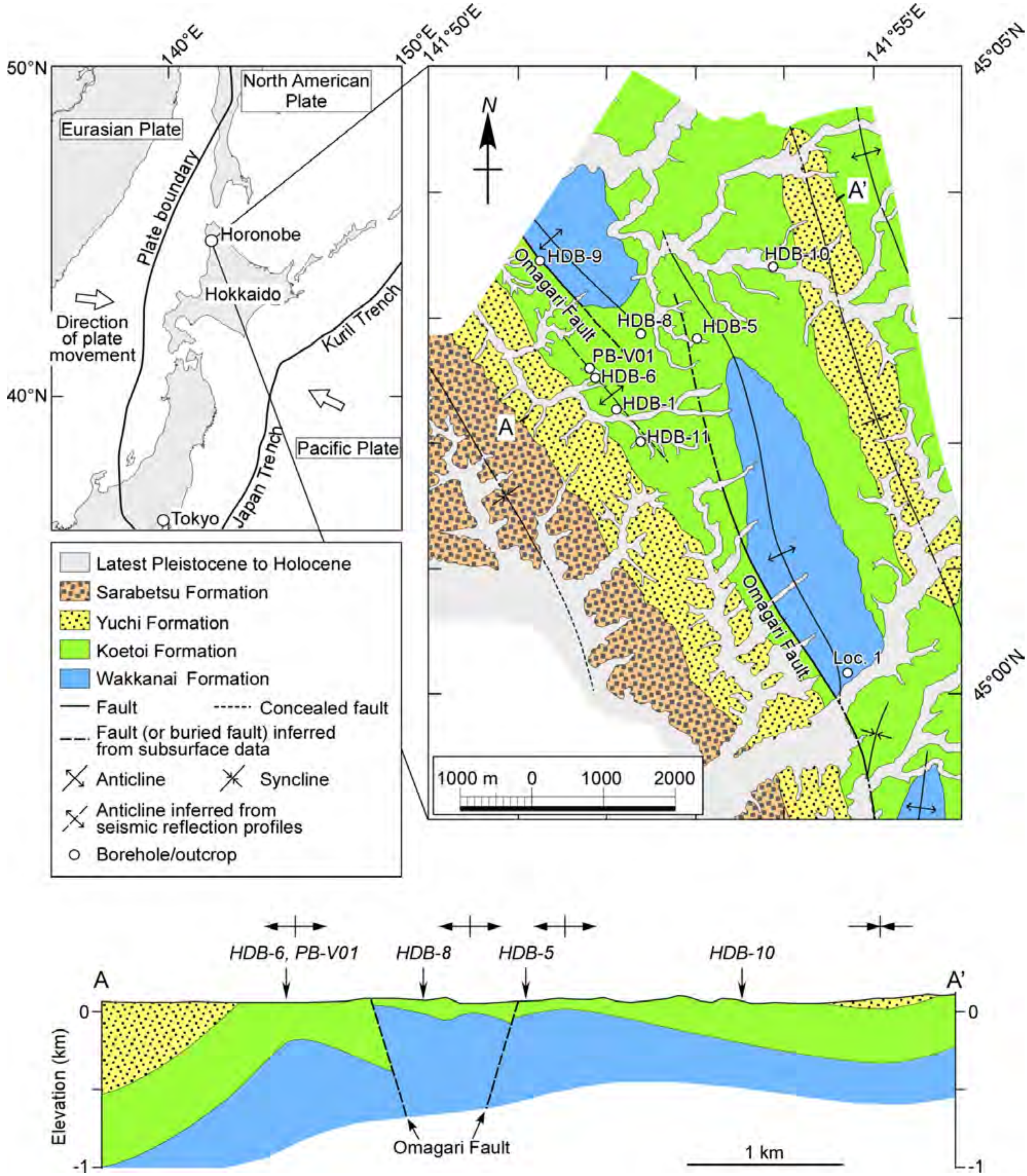

140°E
150°E
141°50'E
141°55'E
45°05'N
45°00'N
50°N
40°N
North American Plate
Eurasian Plate
Plate boundary
Horonobe
Hokkaido
Direction of plate movement
Kuril Trench
Japan Trench
Pacific Plate
Tokyo
N
HDB-9
HDB-10
HDB-8
HDB-5
PB-V01
HDB-6
HDB-1
HDB-11
A
A'
Omagari Fault
Loc. 1
1000 m 0 1000 2000
Latest Pleistocene to Holocene
Sarabetsu Formation
Yuchi Formation
Koetoi Formation
Wakkanai Formation
Fault
Concealed fault
Fault (or buried fault) inferred from subsurface data
Anticline
Syncline
Anticline inferred from seismic reflection profiles
Borehole/outcrop
HDB-6, PB-V01
HDB-8
HDB-5
HDB-10
Elevation (km)
0
-1
Omagari Fault
1 km

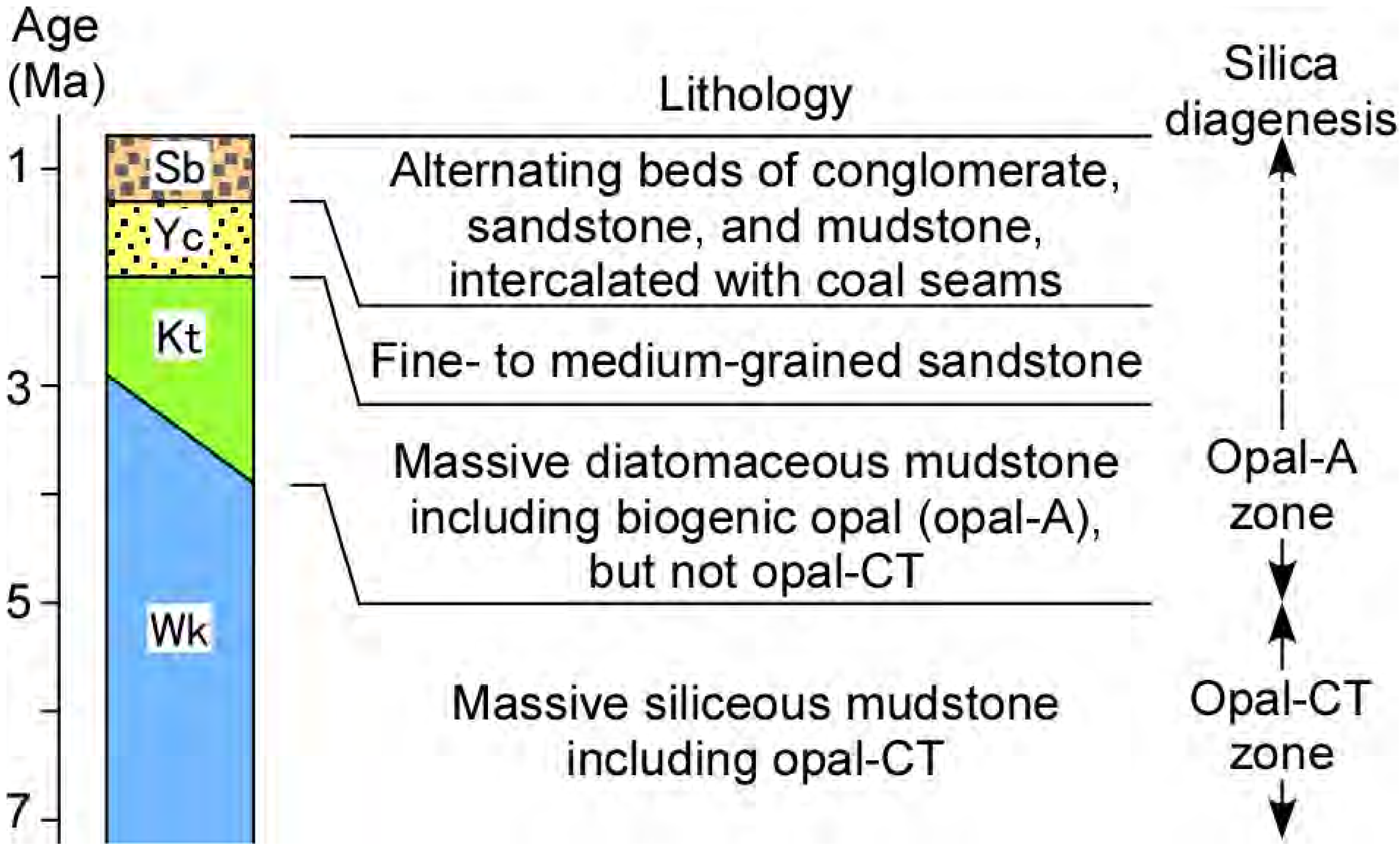

Age
(Ma)
1
3
5
7
Sb
Yc
Kt
Wk
Lithology
Alternating beds of conglomerate, sandstone, and mudstone, intercalated with coal seams
Fine- to medium-grained sandstone
Massive diatomaceous mudstone including biogenic opal (opal-A), but not opal-CT
Massive siliceous mudstone including opal-CT
Silica diagenesis
Opal-A zone
Opal-CT zone

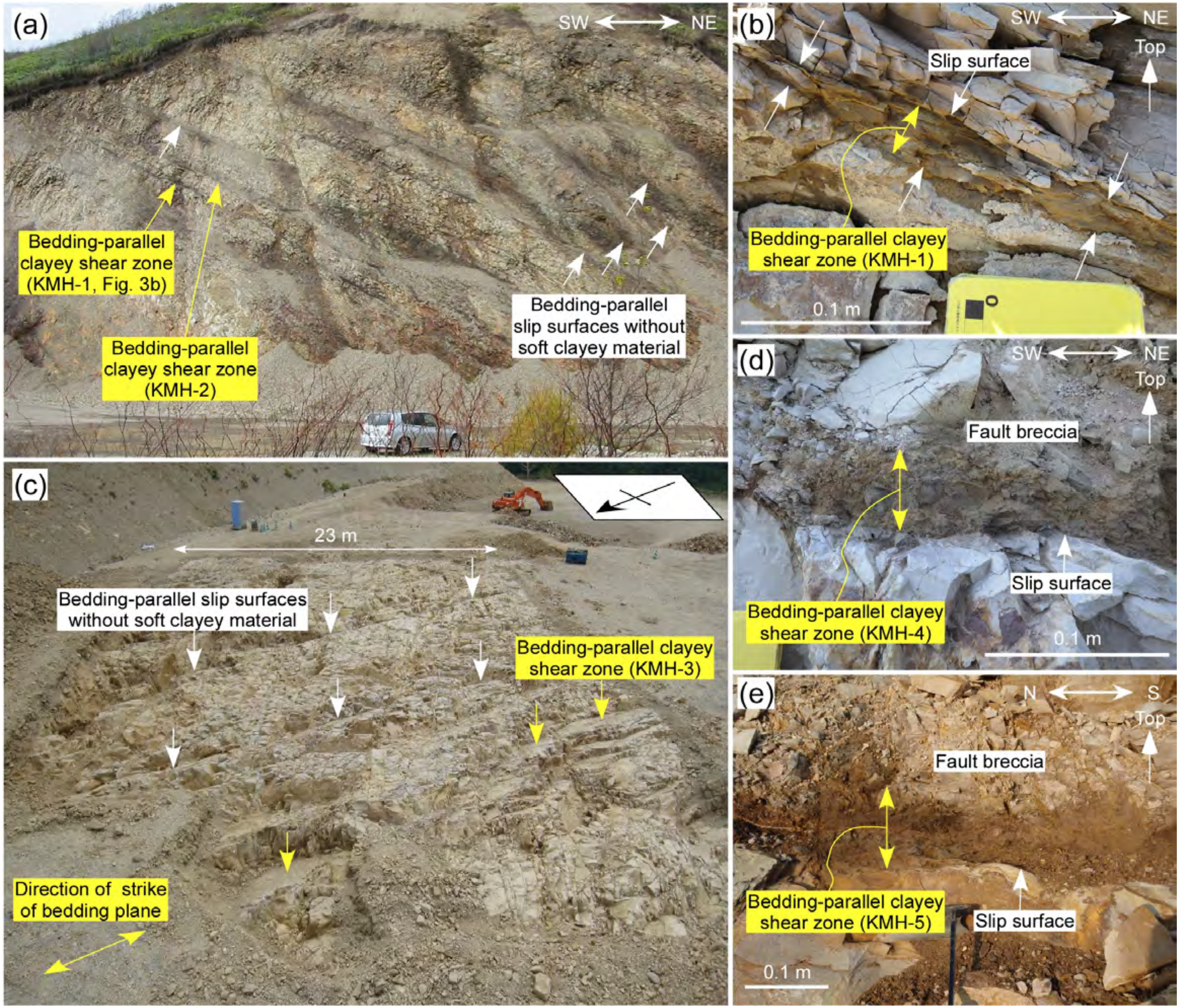
(a)
SW NE
Bedding-parallel clayey shear zone (KMH-1, Fig. 3b)
Bedding-parallel clayey shear zone (KMH-2)
Bedding-parallel slip surfaces without soft clayey material
(b)
SW NE
Top
Slip surface
Bedding-parallel clayey shear zone (KMH-1)
0.1 m
(c)
23 m
Bedding-parallel slip surfaces without soft clayey material
Bedding-parallel clayey shear zone (KMH-3)
Direction of strike of bedding plane
(d)
SW NE
Top
Fault breccia
Slip surface
Bedding-parallel clayey shear zone (KMH-4)
0.1 m
(e)
N S
Top
Fault breccia
Bedding-parallel clayey shear zone (KMH-5)
Slip surface
0.1 m

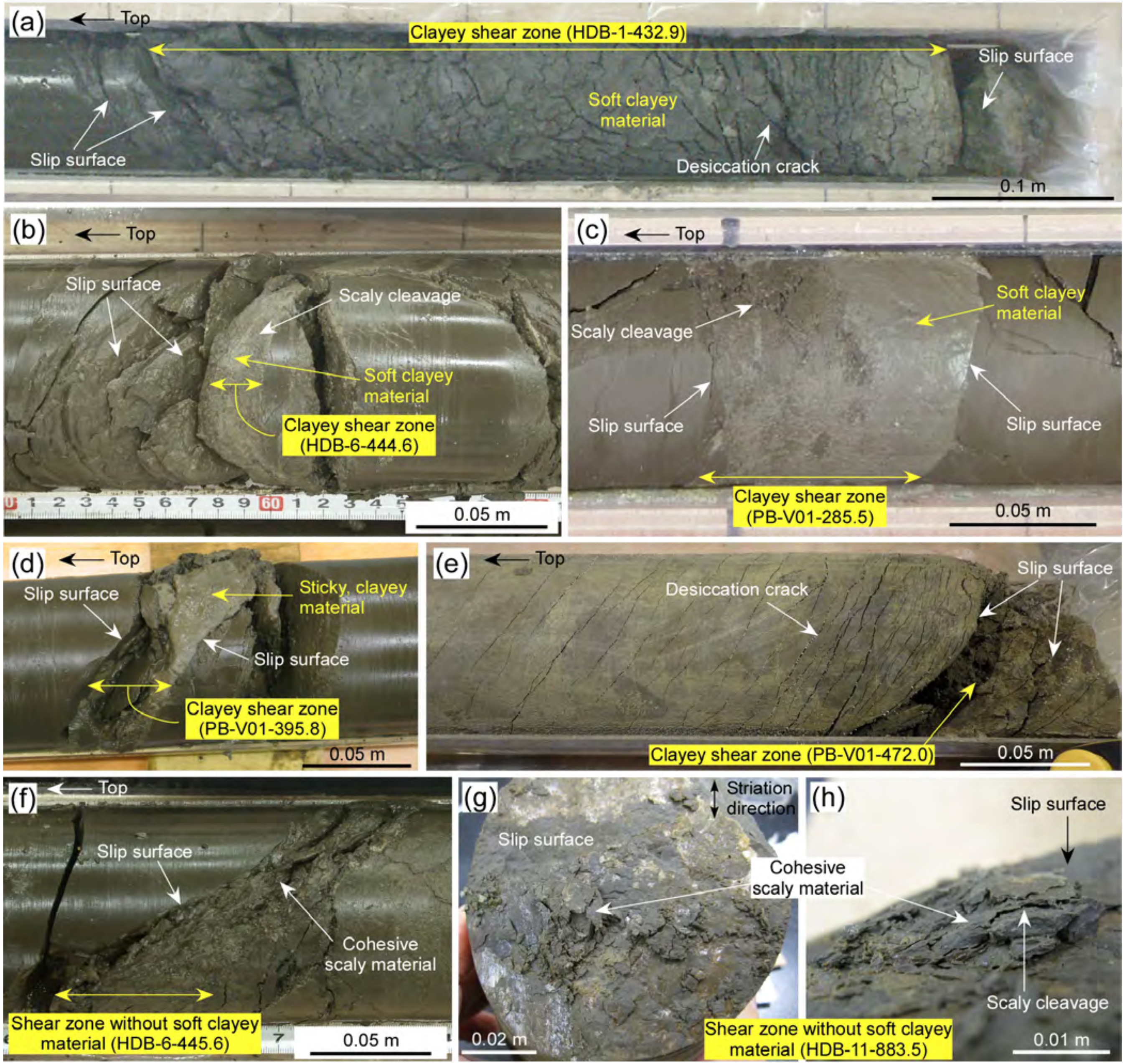

(a)
Top
Clayey shear zone (HDB-1-432.9)
Slip surface
Soft clayey material
Slip surface
Desiccation crack
0.1 m
(b)
Top
Slip surface
Scaly cleavage
Soft clayey material
Clayey shear zone (HDB-6-444.6)
0.05 m
(c)
Top
Soft clayey material
Scaly cleavage
Slip surface
Slip surface
Clayey shear zone (PB-V01-285.5)
0.05 m
(d)
Top
Sticky, clayey material
Slip surface
Slip surface
Clayey shear zone (PB-V01-395.8)
0.05 m
(e)
Top
Slip surface
Desiccation crack
Clayey shear zone (PB-V01-472.0)
0.05 m
(f)
Top
Slip surface
Cohesive scaly material
Shear zone without soft clayey material (HDB-6-445.6)
0.05 m
(g)
Striation direction
Slip surface
Cohesive scaly material
0.02 m
(h)
Slip surface
Scaly cleavage
Shear zone without soft clayey material (HDB-11-883.5)
0.01 m

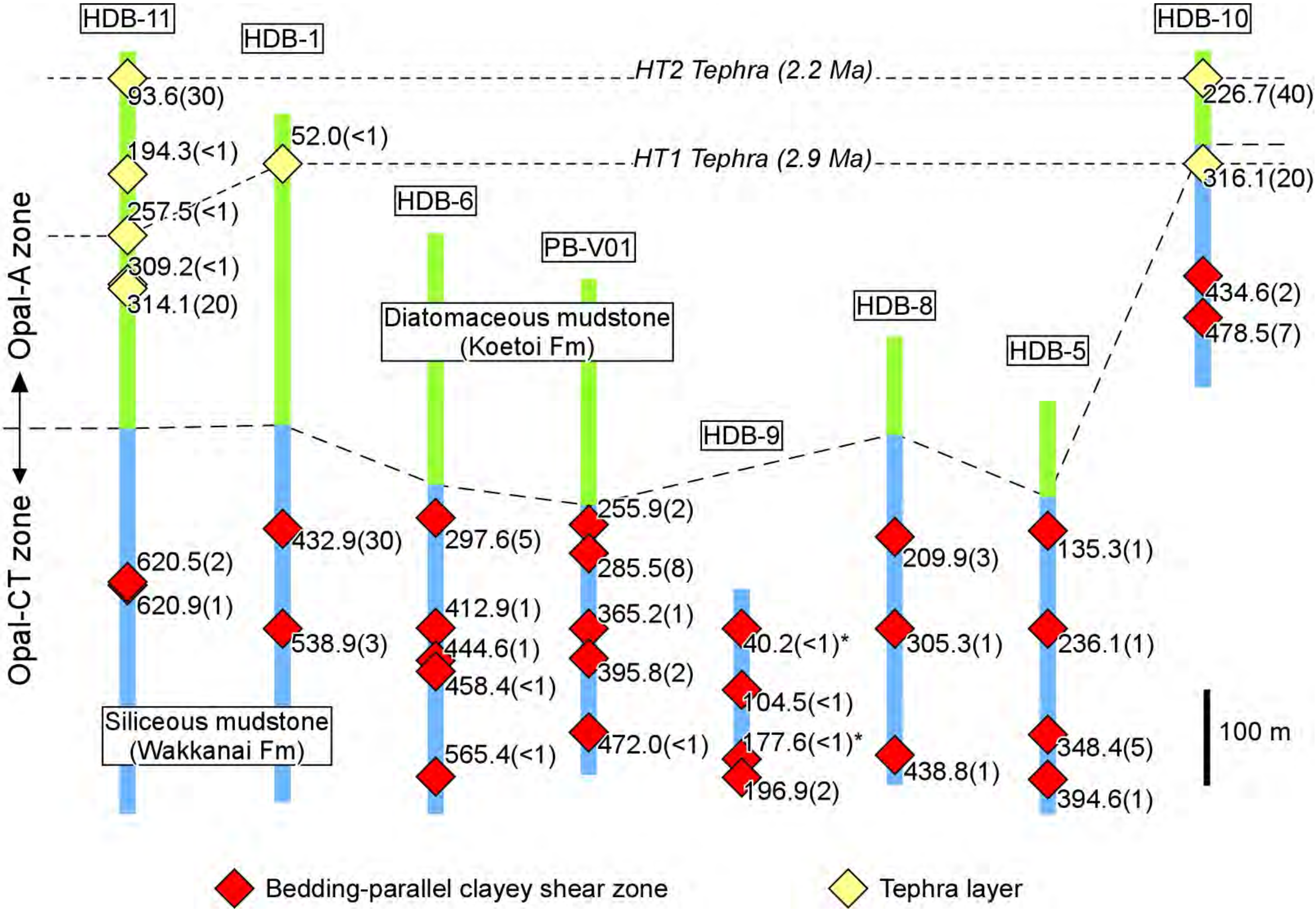
HDB-11
HDB-1
HDB-6
PB-V01
HDB-9
HDB-8
HDB-5
HDB-10
HT2 Tephra (2.2 Ma)
HT1 Tephra (2.9 Ma)
Opal-A zone
Opal-CT zone
Diatomaceous mudstone (Koetoi Fm)
Siliceous mudstone (Wakkanai Fm)
93.6(30)
194.3(<1)
257.5(<1)
309.2(<1)
314.1(20)
620.5(2)
620.9(1)
52.0(<1)
432.9(30)
538.9(3)
297.6(5)
412.9(1)
444.6(1)
458.4(<1)
565.4(<1)
255.9(2)
285.5(8)
365.2(1)
395.8(2)
472.0(<1)
40.2(<1)*
104.5(<1)
177.6(<1)*
196.9(2)
209.9(3)
305.3(1)
438.8(1)
135.3(1)
236.1(1)
348.4(5)
394.6(1)
226.7(40)
316.1(20)
434.6(2)
478.5(7)
100 m
Bedding-parallel clayey shear zone
Tephra layer

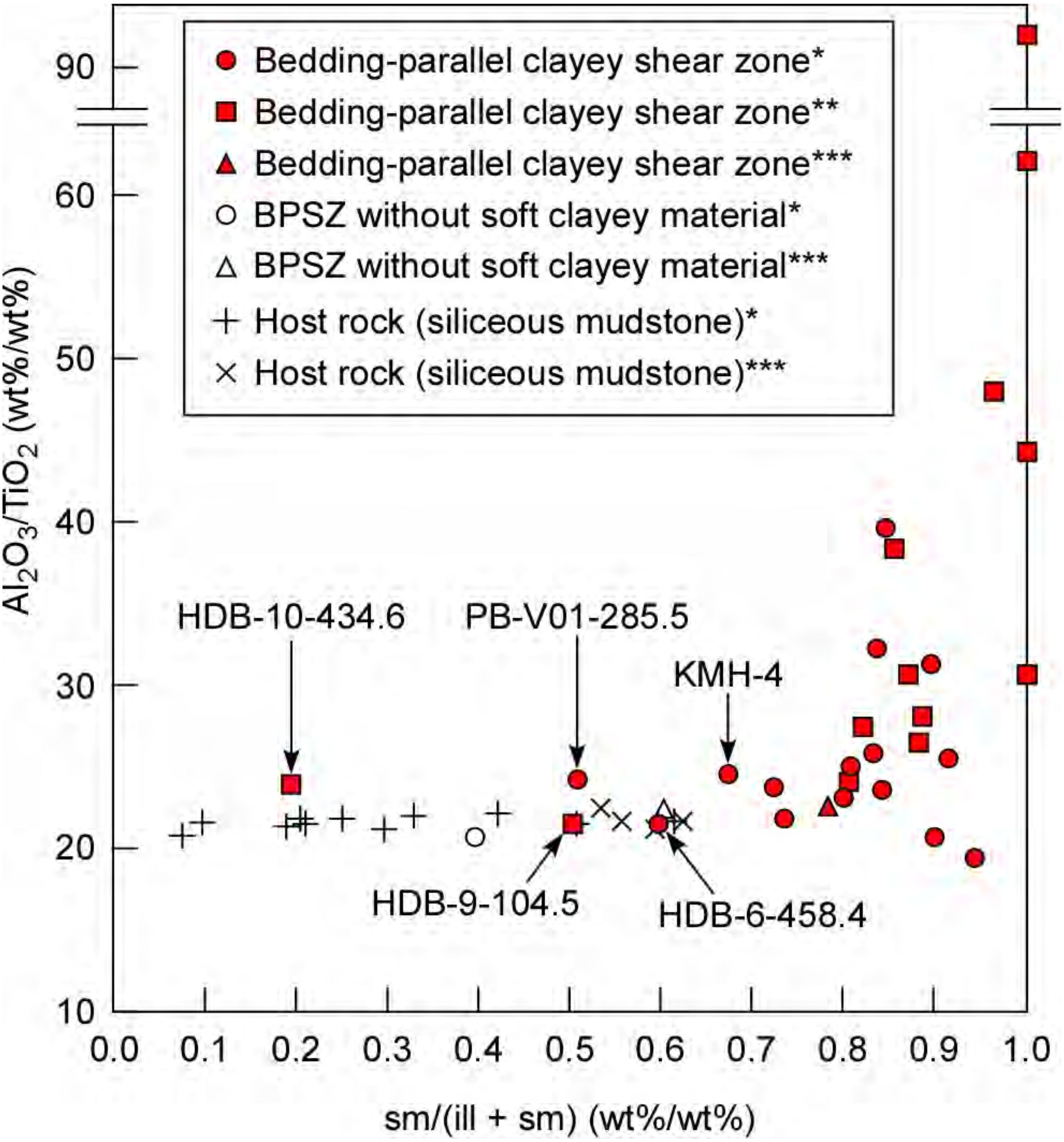

Bedding-parallel clayey shear zone*
Bedding-parallel clayey shear zone**
Bedding-parallel clayey shear zone***
BPSZ without soft clayey material*
BPSZ without soft clayey material***
Host rock (siliceous mudstone)*
Host rock (siliceous mudstone)***
HDB-10-434.6
PB-V01-285.5
KMH-4
HDB-9-104.5
HDB-6-458.4
Al2O3/TiO2 (wt%/wt%)
sm/(ill + sm) (wt%/wt%)
10
20
30
40
50
60
90
0.0
0.1
0.2
0.3
0.4
0.5
0.6
0.7
0.8
0.9
1.0

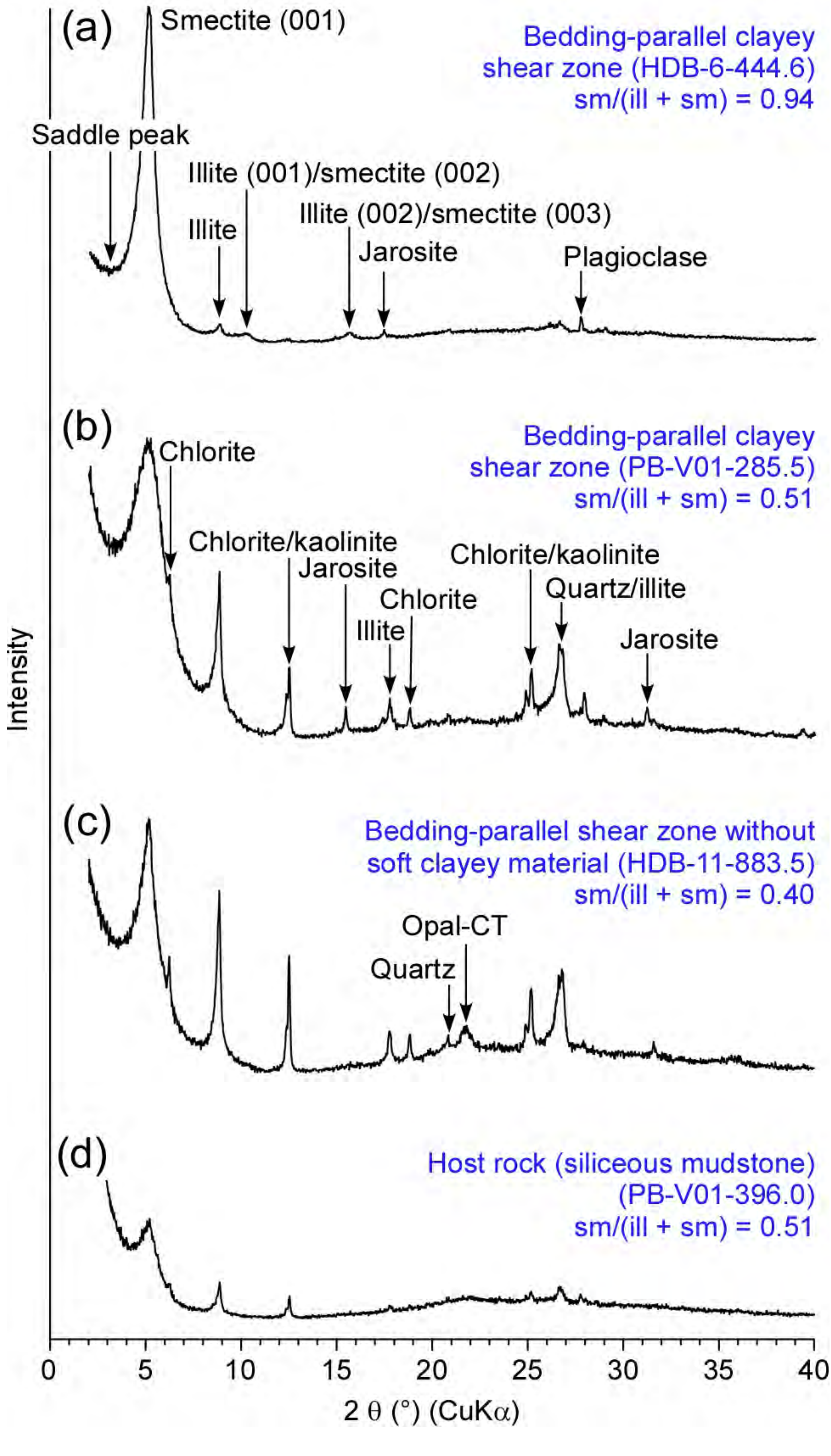

(a)
Smectite (001)
Bedding-parallel clayey
shear zone (HDB-6-444.6)
sm/(ill + sm) = 0.94
Saddle peak
Illite (001)/smectite (002)
Illite
Illite (002)/smectite (003)
Jarosite
Plagioclase
(b)
Chlorite
Bedding-parallel clayey
shear zone (PB-V01-285.5)
sm/(ill + sm) = 0.51
Chlorite/kaolinite
Jarosite
Chlorite/kaolinite
Quartz/illite
Chlorite
Illite
Jarosite
(c)
Bedding-parallel shear zone without
soft clayey material (HDB-11-883.5)
sm/(ill + sm) = 0.40
Opal-CT
Quartz
(d)
Host rock (siliceous mudstone)
(PB-V01-396.0)
sm/(ill + sm) = 0.51
Intensity
0
5
10
15
20
25
30
35
40
2 θ (°) (CuKα)

Table 1 Details of and analytical results for the shear zone and host rock samples analysed in this study.

Sample number	Thickness (m)	sm/(ill + sm) (wt%/wt%)	Al_2O_3/TiO_2 (wt%/wt%)
Bedding-parallel clayey shear zone			
KMH-1	0.02	0.89**	28.15
KMH-2	0.03	1.00**	44.41
KMH-3	0.02	0.86**	38.41
KMH-4	0.03	0.67*	24.52
KMH-5	0.07	0.89*	31.29
HDB-1-432.9	0.3	1.00**	92.09*
HDB-1-538.9	0.03	0.88**	26.54
HDB-5-135.3	0.01	0.87**	30.68
HDB-5-236.1	0.01	0.91*	25.54
HDB-5-348.4	0.05	0.81*	25.00
HDB-5-394.6	0.01	0.83*	25.93
HDB-6-297.6	0.05	0.84*	32.32
HDB-6-412.9	0.01	1.00**	30.68***
HDB-6-444.6	0.01	0.94*	19.39
HDB-6-458.4	<0.01	0.60*	21.61
HDB-6-565.4	<0.01	0.78****	22.71****
HDB-8-209.9	0.03	0.96**	48.00
HDB-8-305.3	0.01	0.82**	27.54
HDB-8-438.8	0.01	0.80**	24.18
HDB-9-104.5	<0.01	0.50**	21.50*
HDB-9-196.9	0.02	0.72*	23.84
HDB-10-434.6	0.02	0.19**	23.92
HDB-10-478.5	0.07	1.00**	62.19
HDB-11-620.5	0.02	0.73*	21.85
HDB-11-620.9	0.01	0.80*	23.09
PB-V01-255.9	0.02	0.85*	39.62
PB-V01-285.5	0.08	0.51*	24.23
PB-V01-365.2	0.01	1.00**	30.68
PB-V01-395.8	0.02	0.90*	20.76
PB-V01-472.0	<0.01	0.84*	23.58
Bedding-parallel shear zone without soft clayey material			
HDB-6-445.6	0.02	0.60****	22.46****
HDB-11-883.5	<0.01	0.40*	20.76
Host rock (siliceous mudstone)			
HDB-6-326.1	-	0.19*	21.42
HDB-6-445.2	-	0.53****	22.43****
HDB-6-447.4	-	0.59****	21.14****
HDB-6-564.2	-	0.62****	21.71****
HDB-6-579.1	-	0.25*	21.91
HDB-8-111.0	-	0.56****	21.70****
HDB-8-197.5	-	0.21*	21.89
HDB-8-440.1	-	0.30*	21.29
HDB-9-72.10	-	0.08*	20.80
HDB-9-223.15	-	0.10*	21.60
HDB-9-321.4	-	0.42*	22.18
HDB-9-519.5	-	0.61*	21.71
HDB-11-598.1	-	0.33*	22.04
PB-V01-396.0	-	0.51*	21.59
PB-V01-518.3	-	0.21*	21.48

*Performed by Hiruzen Inst. for Geol. and Chron. (this study)
**Performed by Earth Science Co. Ltd. (this study)
***Data from Hiraga and Ishii (2008)
****Data from Milodowski et al. (2004)